Energetic Macroscopic Representation of a mechanical compression-assisted hybrid thermochemical cycle exploiting low grade heat for cold applications

Antoine Perrigot, Maxime Perier-Muzet, Pascal Ortega, Franco Ferrucci, Driss Stitou

Energetic Macroscopic Representation of a mechanical compression-assisted hybrid thermochemical cycle exploiting low grade heat for cold applications.

PERRIGOT Antoine[a,*], PERIER-MUZET Maxime[a,b], ORTEGA Pascal [c] , FERRUCCI Franco[c], STITOU Driss[a].

[a] CNRS-PROMES laboratory, Tecnosud, Rambla de la thermodynamique, 66100 Perpignan, France

[b] UPVD Université de Perpignan Via Domitia, 52 Avenue Paul Alduy, 66100 Perpignan, France

[*] Corresponding author : mailto: antoine. perrigot@promes. cnrs. fr

Keywords: Energetic Macroscopic Representation, hybrid thermochemical system, mechanical compression, low grade heat valorization, cold production, thermal energy storage

Abstract

This paper describes an original model based on The Energetic Macroscopic Representation (EMR) to develop a control structure of an innovative compression-assisted hybrid thermochemical cooler driven by low-grade thermal energy. Hybrid thermochemical cooler with mechanical compression have a wider operating temperature range than conventional thermochemical processes. This makes it possible to exploit lower grade heat sources and/or produce cold at lower temperatures. In addition, the ability to control compressor speed increases thermochemical process controllability to respond to load or source variations. Nodal modeling of each process component is developed according to the EMR formalism. A parametric identification and validation of this process model is then carried out using experimental data. The deviation from the experimental data is lower than $1\ bar$ for the reactor, condenser and evaporator pressure, lower than 0.1 for the reaction advancement and lower than $2\ °C$ for the reactor wall temperature. The EMR model is then inverted to obtain a process control law for maintaining a cold room at $-18\ °C$. Despite the variation in cooling demand from a minimum of $100\ W$ to a maximum of $700\ W$, the compressor's control structure was able to regulate its speed of rotation to maintain the cold room temperature at $-18\ \pm 0.5\ °C$ for $24\ h$.

Nomenclature:

Variables

$\Delta_r H\ (J.mol^{-1})$	Enthalpy of reaction
$\Delta_r S\ (J.mol^{-1}.K^{-1})$	Entropy of reaction
$C_v\ (-)$	Flow coefficient of a valve
$\dot{S}\ (J.mol^{-1}.K^{-1}.s^{-1})$	Entropy flow
$c_p\ (J.kg^{-1}.K^{-1})$	Mass heat capacity
$\dot{m}\ (kg.s^{-1})$	Mass flow rate
$\dot{n}\ (mol.s^{-1})$	Molar flow rate
$v_m\ (m^3.mol^{-1})$	Molar volume
$h\ (J.mol^{-1})$	Molar specific enthalpy
$\Phi\ (W)$	Rate of heat flow
$\Omega\ (rpm)$	Compressor rotation speed
$G\ (-)$	Specific density
$H\ (J)$	Enthalpy
$P\ (bar)$	Pressure
$Q\ (J)$	Heat
$R\ (J.K^{-1}.mol^{-1})$	Ideal gas constant
$S\ (J.mol^{-1}.K^{-1})$	Entropy
$T\ (K)$	Temperature
t (s)	Time
$U\ (J)$	Internal energy
$UA\ (W.K^{-1})$	Overall heat transfer coefficient
$V\ (m^3)$	Volume
$X\ (-)$	Advancement of the reaction
$m\ (kg)$	Mass
$n\ (mol)$	Number of moles
$w\ (J)$	Mechanical work
α	Kinetic exponent
$\varepsilon(-)$	Ratio dead/swept volume
$\eta\ (-)$	Efficiency
$\nu\ (-)$	Stoichiometric coefficient

Subscripts and superscripts

°	Standard conditions
htf	Heat transfer fluid
av	Average
kin	Kinetic
$comp$	Compressor
$cond$	Condenser
cc	Compression chamber
dec	Decomposition
dv	Dead volume
eq	Equilibrium
$evap$	Evaporator
exp	Experimental
ext	Exterior
g	Gas
in	Inlet/Input
int	Interior
is	Isentropic
l	Liquid
out	Outlet/Output
r	Reactor
s	Salt
sat	Saturation
sim	Simulation
$synt$	Synthesis
sys	System
w	Wall
cr	Cold room

Acronyms

EMR	Energetic Macroscopic Representation
ENG	Expanded Natural Graphite
$RMSE$	Root Mean Square Error

1. Introduction

1.1. Study framework

Within the framework of the energy transition, thermochemical systems could prove to be an interesting way for valorizing low temperature heat sources (less than 100°C), such as industry thermal waste or low temperature solar heat provided by simple flat plate collectors. In 2016, according to [1], 72% of the primary energy consumption is lost and transformed into heat and 63% of this heat is rejected at a temperature lower than 100 °C. Thermochemical systems allow to obtain different useful effects such as heat upgrading or cold production while also providing a long term storage function with no self-discharge. Basic thermochemical heat transformers are based on the management of a reversible chemical reaction between a reactive salt (the sorbent) and a gas (the sorbate). They are mainly heat driven systems (electricity is only needed to power the circulation pumps for the various heat transfer fluids) and thus allow cold production with low electricity consumption.

Despite this obvious advantage, the most recent research is focused on the hybridization of a such thermochemical systems with a mechanical compressor powered by electricity. This is because the latter allows a wider range of application for thermochemical systems by making it possible to use heat sources at lower temperatures or to produce cold at lower temperatures than basic thermochemical heat transformers. These new hybrid systems allow, for example, to produce heat at 150°C from a heat source available only at 90°C [2], to perform an inter-seasonal storage allowing to heat a house in a cold climate with outside temperature ranging from -5°C to -30°C) [3], to produce heat and cold simultaneously [4], [5], to use and valorize the heat of exhaust gases of a refrigerated truck in order to help maintain the temperature of its cold chamber [6], [7] or to make possible a cold production by recovering the heat generated by a fuel cell or/and an electrolyzer allowing to obtain increase the overall efficiency of the electricity storage/discharge in the form of hydrogen [8].

The original modeling approach of a hybrid compression-assisted thermochemical systems that is proposed here, allows on the one hand to facilitate the implementation and the coupling of this process to

other components that are modelled with the same Energetic Macroscopic Formalism (EMR) and on the other hand makes it possible to obtain control structures for the system which enable the definition of the different control laws to be applied to the system to achieve the desired effect. It is thus possible to set the different control variables (flow rates of heat transfer fluids, compressor rotation speed…) to be applied to the system. Both of these two new features are made possible by using the Energetic Macroscopic Representation (EMR) approach, which is developed and applied for the first time to this kind of thermochemical process.

This paper is structured as follows: part 2 is about the description of the EMR and of a classical thermochemical system. The development of the EMR model which represents the major part of the work is presented in part 3. Part 4 concerns the validation of this model with experimental data. Part 5 presents an example of the use of the EMR model, such as the temperature control strategy of a cold room, whose structure is obtained by inversion of the EMR model. Finally, a conclusion is reached in part 6.

2. EMR and system description

2.1. The Energetic Macroscopic Representation

The Energetic Macroscopic Representation (EMR) is a graphical formalism that allows a synthetic representation of multi-physical energetic systems described in [9]. A systematic deduction of control structures can be achieved if different formalism rules are respected. The EMR design was inspired by other types of system representations such as the Bond graph or the causal informational graph. Developed in 2000 to analyze and control electromechanical systems, the EMR formalism has been extended over the years to cover other energetic domains. To describe physically each of these domains, a pair of kinetic and potential variables is used to respect the action-reaction principle. This principle requires on the one hand, that any subsystem imposing an action on another subsystem receives in return a reaction from the latter and on the other hand, that the product of the action and reaction variables is homogenous to a power. However, for some physical domains such as thermodynamics, it is necessary to have more than 2 variables to qualify the

energy exchange between two subsystems. A further extension has been proposed by Agbli *et al.* [10] to allow the modelling of thermodynamic systems with 3 variables. The different sets of variables that can be used depending on the physical domain considered are summarized in Table 1.

Table 1 : Effort and flow variables that are available in EMR in function of the physical domain considered.

Domain	Potential variable	Kinetic variable	
Electric	Tension [V]	Current [A]	
Translational mechanics	Force [N]	Velocity [$m.s^{-1}$]	
Rotational mechanics	Torque [N.m]	Angular velocity [$rad.s^{-1}$]	
Hydraulics	Pressure [Pa]	Volumetric flow rate [$m^3.s^{-1}$]	
Thermal	Temperature [K]	Entropy flow [$W.K^{-1}$]	
Thermodynamic	Temperature [K]	Pressure [Pa]	Molar flow rate [$mol.s^{-1}$]

In addition to the action-reaction principle, the EMR is based on the principle of integral causality. This can be summarized by the following observation: if any phenomenon, called the cause, generates at a given time another phenomenon, called the effect, then it is impossible for the effect to be preceding the cause. In other terms, the reaction of a subsystem can only occur with a certain delay regarding the action that generated it. The integral causality goes further in the description of physical systems as it imposes then from this integral causality, to describe the outputs of a subsystem has an integral function of the inputs. This is the natural way to describe physical systems because if a derivative causality were used, the system would respond with an infinite power to a step input, which is not the physical response of a real system.

The EMR is based on the description of the energy exchanges between the different components of a complex system. Each component is represented by a given block and different blocks can be used to describe the physics of the system. A source element is used at each bound point to represent a source or sink of power for the system. When a subsystem accumulates energy, an accumulation block is additionally used. A mono-physical coupling block enable the representation of a subsystem submitted to the same energetic domain on both sides. When the domain is different on each side of the subsystem a multi-physical conversion block is then used. The EMR also offers the possibility to represent subsystems submitted to more than 2 energy flows by using several coupling blocks. Finally, with the extension of the EMR towards thermodynamics, several blocs have been added in order to express the power contained in a fluid flow. In order to obtain a control

structure from an EMR model it is necessary to perform an inversion of each of the blocks involved in the control chain. These blocks are represented in blue. All these blocs are given in *Figure 1*.

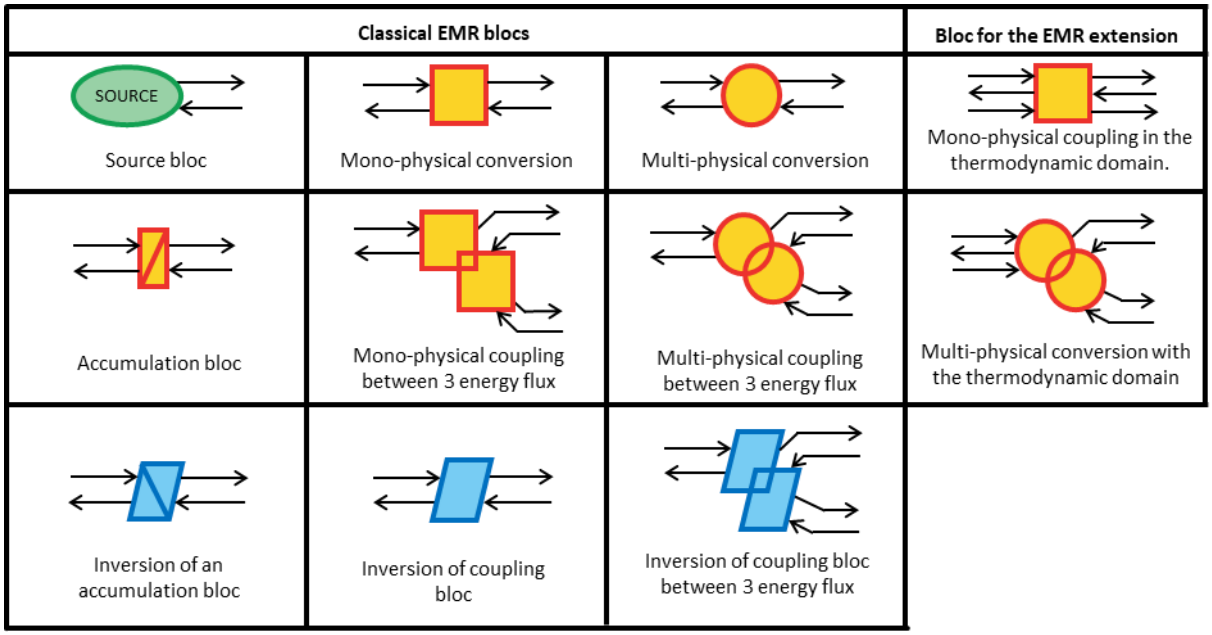

Figure 1 : Blocs available in an EMR model.

The EMR has two major advantages. On the one hand, it allows to easily couple different systems together if they are all modeled according to this formalism. In addition, the EMR enables to easily find a control structure by an inversion method of the model as well as the required number of sensors to be implemented to operate this control. This inversion is only feasible if all the EMR principles have been correctly observed.

Since its initial use for describing electromechanical systems in 2000, the EMR has been applied many times to model complex systems. These include for example a hybrid electric vehicle [11], a wind turbine [12], a subway traction system [13], a diesel internal combustion engine [14], a Stirling engine [15], an electrolyzer [16] or a fuel cell [17]. The EMR model developed in this paper is however the first one developed for a solid/gas thermochemical system.

2.2. Thermochemical systems

Thermochemical systems can be used to store and valorize low-grade waste heat for later production of higher temperature heat (heat upgrading) or cooling. The modeling presented in this paper is intended for a

cold production system, but only a few modifications would be necessary to model a thermochemical heat transformer process. A thermochemical sorption system is based on the thermal effect of the reversible solid-gas reaction shown by equation (1). For this modeling, the reaction between a salt and a reactive gas takes place in a single fixed-bed reactor that exchanges the reactive gas with an evaporator or a condenser according to the direction of the reaction:

$$S_0 + \nu . G \underset{dec}{\overset{synt}{\rightleftarrows}} S_1 + \nu . \Delta_r H^\circ \quad (1)$$

The left to right direction in equation (1) corresponds to the synthesis phase where one mole of the desorbed salt (S_0) reacts with ν moles of gas (G) to form the synthesized salt (S_1). $\Delta_r H^\circ$ is the standard enthalpy of reaction and corresponds to the rejected heat when a mole of gas is absorbed by the salt during the synthesis reaction. The right to left direction corresponds to the decomposition phase, which is an endothermic reaction. This reaction is monovariant so if one intensive parameter is fixed, temperature or pressure for example, the other is set by the equilibrium state. The equilibrium can be described in a first approximation with the Clausius-Clapeyron equation as shown in (2) and described by [18].

$$P_{eq} = P_{ref} . \exp\left(\frac{\Delta_r H^\circ}{R} - \frac{\Delta_r S^\circ}{R . T_{eq}}\right) \quad (2)$$

In this equation, P_{eq} is the equilibrium pressure of the reaction taking place at the temperature T_{eq}. $\Delta_r H^\circ$ and $\Delta_r S^\circ$ represent respectively the enthalpy and entropy of reaction in the standard conditions ($P_{ref} = 1$ bar and $T_{ref} = 25°C$). Thermodynamic constraints in pressure and temperature different from those corresponding to equilibrium must be imposed on the reactor for the reaction to take place.

A conventional thermochemical system with fixed-bed reactor operates according two distinct phases and consists of 5 main components: a reactor, a condenser, a tank, an expansion valve and an evaporator. During the storage phase, also called decomposition phase, the thermal energy from the hot source (Q_{dec}) is transferred to the reactor to raise its temperature. The reactor being closed, the temperature increases up to the temperature of the hot source T_{hot} and leads to a pressure increase due to the monovariant equilibrium

of the reaction. This equilibrium is described by equation (2)(21). When the pressure in the reactor reaches the condenser pressure, these two components are then connected. The pressure in the reactor is thus fixed by the condenser and its temperature is conditioned by the heat exchange with the hot source. The reactant is put out of equilibrium and the decomposition reaction takes place: the gas is desorbed and flows towards the condenser. In the condenser, the gas is cooled down to the saturated vapor state (desuperheating of the vapors) and then condenses. These two phenomena imply that a quantity of heat (Q_{cond}) must be evacuated towards the environment sink. The resulting liquid is stored at ambient temperature in the liquid tank.

Before the cold production phase, also known as the synthesis phase, the valve connecting the reactor to the rest of the system is closed to isolate it. The reactor is cooled by a heat transfer fluid to lower its pressure. When the pressure drops below that of the evaporator, the reactor is connected to the evaporator. The gas is then chemically absorbed by the reactive salt producing a heat of reaction (Q_{synt}) that is released to the environment. This chemical reaction between the gas and the reactive salt causes a decrease in pressure at the evaporator and, to compensate for this decrease in pressure, the liquid in the evaporator vaporizes, inducing an endothermic effect at temperature T_{cold}. The liquid in the tank is then expanded to the vaporization pressure to feed the evaporator. The endothermic nature of evaporation allows heat to be absorbed from the cold source (Q_{evap}), which is the desired useful effect.

Scientific research has focused on hybrid thermochemical systems using a compressor for several years now. This enables to recover heat at a lower temperature than conventional systems [19], [20] or to produce cold at a lower temperature [21]. The compressor can be used independently in the two phases of operation of the thermochemical system. The operating of such hybrid thermochemical systems is described in Figure 2. In this figure, Q_{cond}, Q_{evap} , Q_{dec} and Q_{synt} represent the heat exchanged in the condenser, evaporator and reactor respectively, depending on whether the phase is decomposition or synthesis. The compressor in the decomposition phase allows the pressure of the reactor (P_{dec}) and the condenser (P_{cond}) to be decoupled thanks to a mechanical work (W_{comp}^{dec}). The reactor can therefore desorb the gas at a lower temperature T'_{hot} than would be required if the reactor were directly connected to the condenser (T_{hot}). This allows the reactor

to operate at a lower pressure that of the condenser and the compressor allows the gas to flow towards the condenser by overcoming the pressure difference. In the synthesis phase, the compressor allows the evaporation pressure (P_{evap}) to be decoupled from the reactor pressure (P_{synt}) thanks to the mechanical work (W_{comp}^{synt}) and thus the evaporation pressure to be reduced. The cold is thus produced at a lower temperature T'_{cold}.

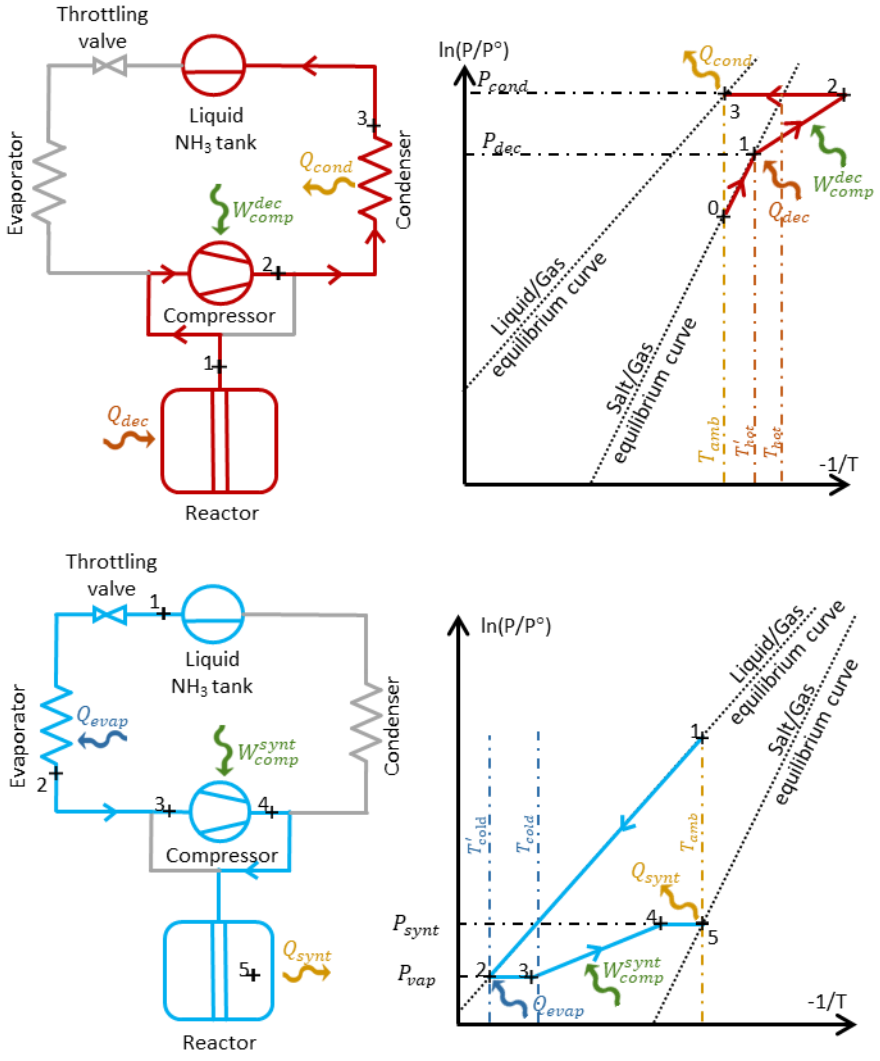

Figure 2 : Description of the 2 proposed compressor configurations: the assisted decomposition on top and the assisted synthesis below.

Several types of modeling for thermochemical fixed bed reactor have been developed in the scientific literature. The first one was developed from the description of a small volume of salt and described the heat

and mass transfers at this local scale [22]. At each point of the reactor the pressure, the temperature and the advancement of the reaction is available thanks to the resolution of differential equations resulting from heat and mass balance. These types of models enable to show the existence of two reaction fronts more or less diffused. The first one is relative to the heat transfer inside the reactive bed and the second one to the mass transfer. This type of model enables a detailed understanding of the phenomenon at a small scale but requires the knowledge of many data related to the material and difficult to access. To make the computation of this model easier, a simplification of this model has been proposed by considering sharp reactive fronts [23]. It has also been shown in [24] that if pressure is high enough in the reactor (greater than 0.5 bar) to prevent kinetics limitations or if the permeability of the reactive bed is high enough, then the mass transfer no longer limits the reaction rate and the pressure can then be assumed to be uniform in the reactor. Finally, a last simplification can be made by assuming that the temperature is also uniform in the reactor. This simplification can be made if Expanded Natural Graphite (ENG) is used to find an optimization between heat and mass transfers inside the reactor. This latter type of simplified model of fixed-bed solid/gas reactor is used here to develop the EMR of the thermochemical system.

3. EMR of a hybrid thermochemical system

3.1. EMR of the solid/gas thermochemical reactor

The fixed-bed reactor, depicted on Figure 3 consists of a metallic envelop in which is contained a porous reactive material composed of a compressed composite of salt and expanded natural graphite (GNE) allowing to improve both the diffusion of the reactive gas and the heat transfer. The reactor tube wall is subjected to heat exchange with a heat transfer fluid, which is usually either air or water flowing. Gas diffusers are located in the reactive composite to distribute axially the reactive gas all along the reactor. The dead volume, which represents the volume of the reactor that is not occupied by the reactive composite, is therefore composed of the volume of the diffusers, the free volume of the reactor not occupied by the reactive bed as well as the void volume constituting the porosity of the reactive composite material.

The EMR modeling being based on a macroscopic scale of the energy transfers between the different subsystems, the reactor is considered as a set of 3 subsystems: the reactor wall, the reactive composite and the dead volume. Several assumptions are made to simplify the thermochemical reactor modeling:

- The heat transfer between the dead volume and the reactor tube wall is neglected.
- The reactor shell is assumed to be thermally insulated and therefore does not exchange heat with the environment but only with the heat transfer fluid.
- The temperature and pressure are assumed to be uniform in the reactor.
- Kinetic and potential energy variations are neglected.
- The thermal capacities of the different materials are taken constant whatever the operating temperature.
- All solids (wall and reactive composite) are assumed to be inexpansible and indilatable.

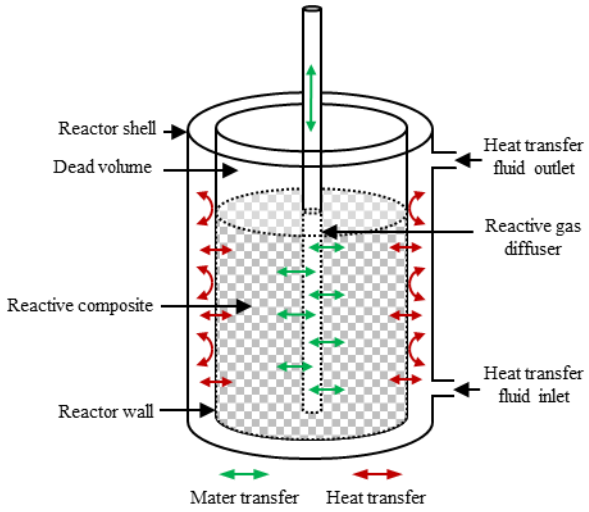

Figure 3 : Scheme of the reactor composed of the 3 subsystems (reactor tube wall, reactive composite and dead volume).

The reactor environment is composed of two sources. On the one hand it is subjected to a thermal exchange between the heat transfer fluid and the reactor tube wall and, on the other hand, to a gas exchange through the top of the diffuser with the other components of the system (evaporator, condenser or

compressor). These exchanges with the sources require the knowledge of the temperature of the heat transfer fluid and the molar flow of gas exchanged between the reactor and the rest of the system.

The wall of the reactor tube as well as the reactive composite itself can accumulate thermal energy, the dead volume can accumulate a certain quantity of gas. There are thus 3 energy accumulators in this system, which will ultimately correspond to 3 state variables for the reactor model and thus 3 accumulation blocs in the EMR model. A schematic representation of these different blocks to be designed, with their thermal or mass interactions is shown in Figure 4.

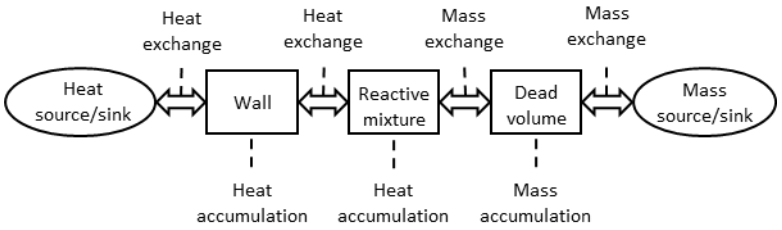

Figure 4 : Scheme of the different subsystems representing the reactor and the different energy exchanges between them.

From these considerations it is possible to design the EMR diagram of the reactor with the different blocs that compose it as well as the different variables representing the energy exchanges. The complete EMR scheme of the reactor is described in Figure 5. The various variables shown in this figure are described below as they appear in the equations describing the behavior of the various blocks. It is also possible to refer to the nomenclature to find the meaning of each variable if required.

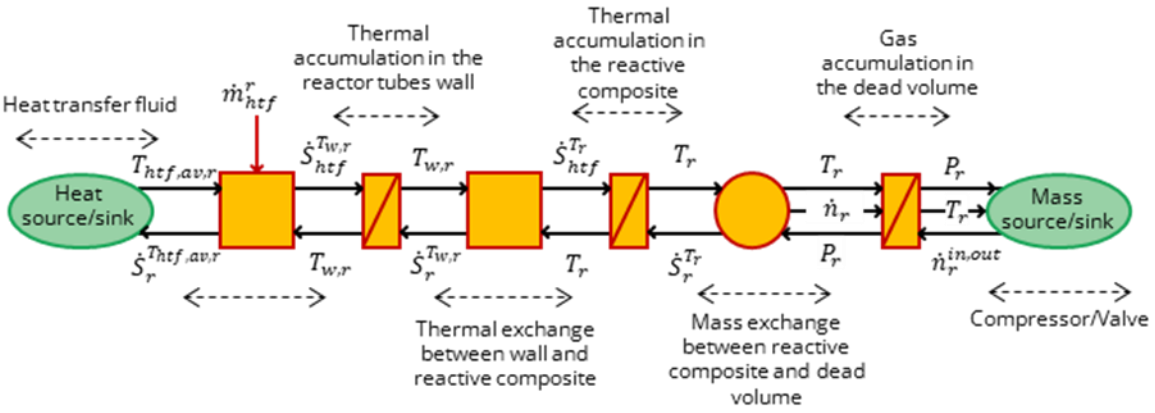

Variables		Subscripts and superscript	
T	Temperature	htf	Heat Transfer Fluid
P	Pressure	av	Average
$\dot{n}$	Molar flow rate	r	Reactor
$\dot{S}$	Entropy flow	w	Wall
$\dot{m}$	Mass flow rate		

Figure 5 : EMR representation of the reactor.

3.1.1. Heat exchange between the heat transfer fluid and the tube reactor wall

The block representing the heat exchange between the heat transfer fluid and the tube reactor wall is a monophysical conversion block as depicted on Figure 5. The inputs are the mean temperature of the heat transfer fluid $T_{htf,av,r}$ and the reactor wall T_w. The outputs are the entropy fluxes associated to the heat exchange $\dot{S}_r^{T_{htf,av}}$ and $\dot{S}_{htf}^{T_w}$.

The entropy fluxes are computed as the ratio between the thermal power exchanged between the heat transfer fluid and the tube reactor wall $\Phi_{w,htf}$ and the considered temperature as shown by equations (3) and (4).

$$\dot{S}_r^{T_{htf,av}} = \frac{\Phi_{w,htf}}{T_{htf,av,r}} \tag{3}$$

$$\dot{S}_{htf}^{T_w} = \frac{\Phi_{w,htf}}{T_w} \tag{4}$$

The thermal power can be expressed from the knowledge of a heat exchange coefficient $(UA)_{r,ext}$ and the average logarithmic temperature difference between the heat transfer fluid and the wall. It's assumed that the temperature difference between the inlet and outlet of the heat transfer fluid is small thus the average logarithmic temperature difference can be estimated as a first approximation by the difference between the average temperature of the heat transfer fluid and the wall temperature. The heat flux can thus be expressed using the equation described by equation (5).

$$\Phi_{w,htf} = (UA)_{r,ext}.(T_{htf,av,r} - T_w) \quad (5)$$

The estimation of the overall heat exchange coefficient is not trivial because of the complex geometry of the heat exchanger. For this reason, it is calculated as a power function of the heat transfer fluid flow rate $\dot{m}_{htf}^{r}$ using a multiplier constant A that is determined by identification from experimental observations. The exponent is determined from the Nusselt correlations found in the literature. The final expression is given by equation (6).

$$(UA)_{r,ext} = A.\left(\dot{m}_{htf}^{r}\right)^{0.6} \quad (6)$$

3.1.2. Heat accumulation in the tube reactor wall

The block that represents the thermal accumulation in the reactor wall is an accumulation block that receives two entropy flows, one coming from the heat transfer fluid $\dot{S}_{htf}^{T_{w,r}}$ and the second from the reactive composite $\dot{S}_{r}^{T_{w,r}}$. This block output is the state variable $T_{w,r}$. This temperature is calculated from a heat balance on the reactor wall based on the thermal mass of the reactor wall $\left(m.c_p\right)_{w,r}$ as shown by equation (7).

$$\left(m.c_p\right)_{w,r}.\frac{dT_{w,r}}{dt} = \left(\dot{S}_{htf}^{T_{w,r}} - \dot{S}_{r}^{T_{w,r}}\right).T_{w,r} \quad (7)$$

A first order differential equation is obtained. The block output $T_{w,r}$ is expressed as an integral function of the inputs (entropy flows). The integral causality imposed by the EMR formalism is thus respected.

3.1.3. Heat exchange between the reactor wall and the reactive composite

This heat exchange is slightly different from the exchange between the heat transfer fluid and the wall because here a heat exchange at the surface contact between two solids. By defining an overall heat exchange coefficient $(UA)_{r,int}$, characterizing a contact conductance between the wall and the reactive composite, it is possible to estimate the heat flux $\Phi_{w,r}$ from the input data of the block that are the reactor wall temperature $T_{w,r}$ and the reactive mixture temperature T_r as shown in equation (8). The overall heat transfer coefficient will be estimated using an identification from experimental observations because there is no correlation to compute it.

$$\Phi_{w,r} = (UA)_{r,int}.(T_{w,r} - T_r) \tag{8}$$

The expression of the entropy flux is then obtained in a similar way to what has been presented in the equation (3)

3.1.4. Heat accumulation in the reactive composite

The block representing the thermal accumulation in the reactive composite is a block with two entropy flows as inputs. The first one comes from heat exchange with the tube reactor wall $\dot{S}_{htf}^{T_r}$ and the second one from the decomposition or synthesis reaction taking place within the reactive composite $\dot{S}_r^{T_r}$. These two entropy flows are obtained using a first principle balance on the reactive composite as shown in equation (9). In this balance, it is essential to note that the sensible heat of the gas arriving in the reactor during the synthesis is neglected. This approximation allows to simplify the EMR modeling while remaining an acceptable assumption since the sensible heat is weak in front of the reaction heat because the gas arrives in the reactor at a temperature relatively close to it.

$$\frac{dU_{s+\mathrm{ENG}}}{dt} = (UA)_{r,int}.\left(T_{w,r} - T_r\right) + \dot{n}_r.h_g(T_r) \tag{9}$$

In this equation, $U_{s+\mathrm{ENG}}$ represents the internal energy of the salt and the ENG, $T_{w,r}$ and T_r refers respectively to the reactor wall temperature and the reactive mixture temperature, $\dot{n}_r$ refers to the molar flow rate of gas consumed (synthesis) or produced (decomposition) the chemical reaction and h_g is the molar enthalpy of the gas. The flow rate is considered positive for the synthesis reaction. It is possible to express this

flow rate from the variation of the reaction advancement X and the total number of moles of salt in the reactant n_s by equation (10).

$$\dot{n}_r = \nu . n_s . \frac{dX}{dt} \tag{10}$$

Where ν is the stoichiometric coefficient of the reaction, i.e. the number of moles of desorbed gas by moles of reactive salt.

Since the internal energy of the reactive mixture U_{s+ENG} is an extensive state variable, it can be expressed as the sum of the internal energy of the salt U_s and the expanded natural graphite U_{ENG} as presented by the equation (11).

$$\frac{dU_{s+ENG}}{dt} = \frac{dU_s}{dt} + \frac{dU_{ENG}}{dt} \tag{11}$$

The case of expanded natural graphite is rather simple because it is possible to assume it as an incompressible and inexpansible solid. With the knowledge of the thermal mass of the ENG $\left(\mathrm{m}. c_p\right)_{ENG}$ and the reactive mixture temperature T_r equation (12) enable the computation of the internal energy of the ENG U_{ENG} .

$$\frac{dU_{ENG}}{dt} = \left(m. c_p\right)_{ENG} . \frac{dT_r}{dt} \tag{12}$$

For the salt, it is necessary to consider its composition (proportion of charged salt and discharged salt) which varies in time according to the advancement of reaction X. To express the internal energy of salt U_s it is preferable to go through the calculation of its enthalpy H_s because in the case where the salt is considered as an incompressible and inexpansible solid it is possible to consider that $dH_s = dU_s$. The enthalpy of the salt can then be decomposed as a function of the molar enthalpy of the charged salt h_1 and the discharged salt h_0 in gas considering as shown in equation (13) where n_s represents the total number of salt.

$$H_s = n_s . [\mathrm{h}_0 . (1 - X) + h_1 . X] \tag{13}$$

The enthalpy of reaction ΔH_r is defined as the thermal energy released by the absorption of one mole of gas during the synthesis reaction. This can be expressed by looking at the reaction expression (1). Equation

(14) is thus obtained where h_0 and h_1 represent respectively the molar enthalpy of the discharged and charged salt, ν is the stoichiometric coefficient of the reaction and h_g the molar enthalpy of the gas involved in the reaction.

$$\Delta_{\mathrm{r}}H = \frac{h_0 - h_1 + \nu . h_g}{\nu} \tag{14}$$

The enthalpy of reaction $\Delta_{\mathrm{r}}H$ depends on the pressure and the temperature at which the reaction is carried out but it is usual, taking into account the relatively weak amplitudes of temperature and pressure undergone by the thermochemical process, to make the assumption that the enthalpy of reaction is constant, and equal to the enthalpy of reaction in the normal conditions of pressure and temperature ($P° = 1\ bar$ and $T° = 25\ °C$). This defines the standard enthalpy of reaction $\Delta_r H°$.

Some assumptions allow to simplify the differentiation of the expression of the salt enthalpy H_s :

- The discharged salt S_0 can be assimilated to an indilatable and incompressible solid: $dh_0 = c_{p,0}.dT_r$. Where h_0 is the molar enthalpy of the discharged salt, $c_{p,0}$ the molar thermal capacity of the discharged salt and T_r the temperature of the reactive mixture.
- The gas can be assimilated to an ideal gas: $dh_g = c_{p,g}.dT_r$. In this equation, h_g is the molar enthalpy of the gas, $c_{p,g}$ the molar thermal capacity of the gas and T_r the temperature of the reactive mixture.
- The enthalpy of reaction $\Delta_r H°$ is assumed to be constant as a function of temperature and pressure: $d\Delta_r H° = 0$

With these assumptions and thanks to equation (14), the differentiation of equation (13) gives the equation (15).

$$\mathrm{dU_s} = n_s.\left[(\mathrm{c_{p,0}} + \nu . X . c_{p,g}\ ).dT_r + \nu.\left(h_g - \Delta_{\mathrm{r}}H°\right).dX\right] \tag{15}$$

In this equation, U_s is the internal energy of the salt, n_s the number of moles of salt, $c_{p,0}$ the molar thermal capacity of the discharged gas, ν the stoichiometric coefficient, X the reaction advancement, $c_{p,g}$ the molar thermal capacity of the gas, h_g the molar enthalpy of the gas and $\Delta_r H°$ the standard enthalpy of the reaction.

An additional assumption is made on the thermal mass of the reactive salt which is taken equal to the average thermal mass of the salt $c_{p,s,av}$ as shown in equation (16).

$$n_s.\left(\mathrm{c_{p,0}} + \nu.X.c_{p,g}\right) = n_s.c_{p,s,av} \tag{16}$$

By combining equations (12), (15) and (16) and after simplification the balance equation on the reactive composite is expressed by equation (17).

$$(\mathrm{n}_s.\mathrm{c_{p,s,av}} + m_{ENG}.c_{p,ENG}).\frac{dT_r}{dt} = (UA)_{r,int}.\left(T_{w,r} - T_r\right) - \dot{n}_r.\Delta_\mathrm{r}H° \tag{17}$$

This equation reflects the fact that the temperature increases of the reactive composite (term on the left hand side of the equal sign) is due on the one hand to the heat exchange with the wall (first term on the right hand side of the equal sign) and, on the other hand, to the quantity of heat absorbed or rejected by the chemical reaction (second term on the right hand side of the equal sign).

To respect the EMR formalism, it is necessary to express the temperature of the reactor as a function of the two entropy fluxes supplied by the adjacent blocs. Thanks to the previous equation, it is possible to identify these 2 entropy fluxes: one due to the heat exchange at the wall of the reactor $\dot{S}_{htf}^{T_r}$, the other due to the heat of by reaction $\dot{S}_r^{T_r}$. These entropy fluxes are expressed by the following equations (18) and (19).

$$\dot{S}_r^{T_r} = -\frac{\dot{n}_r.\Delta H_r°}{T_r} \tag{18}$$

$$\dot{S}_{htf}^{T_r} = \frac{(UA)_{r,int}.(T_{w,r} - T_r)}{T_r} \tag{19}$$

By inserting the equations described by (18) into balance equation (17), the temperature of the reactive composite is expressed as an integral function of the entropy flows that are the inputs of this bloc.

3.1.5. Mass exchange between the reactive composite and the dead volume

The coupling between the thermal part and the fluidic part is done through a multiphysics coupling block in which the inputs of the block are used to express the entropy flow $\dot{S}_r^{T_r}$ using equation (18). To express the

flow of gas absorbed or released by the reactive composite it is necessary to know the variation of the rate of advancement, and thus to introduce a kinetic law.

Several kinetic laws have been proposed in the scientific literature, which are determined either from balances on the reactive composite as in the article by Neveu $et\ al.$ [25] or empirically from experimental observations. This second method has been chosen here because many phenomena influence the kinetic, and it is difficult to account for them by putting them into equations. The chosen kinetic law results from the following considerations: the kinetics of the reaction depends mainly on the deviation from the equilibrium and the current progress of the reaction. Expression (20) from the article by Mazet *et al.* [26] is retained. In this equation X is the reaction advancement, k_{kin} a kinetic coefficient and α an exponent which makes it possible to account for the dependence of the kinetics on the advancement ($\alpha \in [0; 2]$), P_r and T_r the reactor pressure and temperature and $P_{eq}(T_r)$ the equilibrium pressure at the reactor temperature.

$$\frac{dX}{dt} = k_{kin}.X^{\alpha}.\ln\left(\frac{P_r}{P_{eq}(T_r)}\right) \tag{20}$$

This expression is only valid in decomposition. For the synthesis, the term X will be replaced by $(1 - X)$. The equilibrium pressure is calculated with the Clausius-Clapeyron equation (21).

$$\mathrm{P_{eq}(T)} = \mathrm{P^{\circ}}.\exp\left(\frac{\Delta_r \mathrm{H^{\circ}}}{\mathrm{R}} - \frac{\Delta_r S^{\circ}}{\mathrm{R.T}}\right) \tag{21}$$

In this equation $P_{eq}(T)$ is the equilibrium pressure at the considered temperature T, $P°$ is the reference pressure ($P° = 1\ bar$), $\Delta_r H°$ and $\Delta_r S°$ are respectively the standard enthalpy and entropy of the reaction and R is the universal constant of perfect gases.

3.1.6. Mass accumulation in the dead volume

The amount of gas in the dead volume $\dot{n}_{g,dv}$ can be calculated from a mass balance on the dead volume of the reactor. Indeed, this volume is subject to two flows of gas, on the one hand the one produced or absorbed by the reactive salt $\dot{n}_r$ and, on the other hand, the one which is exchanged with the outside $\dot{n}_r^{in,out}$. The quantity of gas in the dead volume can thus be expressed according to (22).

$$\frac{dn_{g,dv}}{dt} = \dot{n}_r + \dot{n}_r^{in,out} \quad (22)$$

The reactor pressure is computed by assuming that the gas behaves like an ideal gas. This approximation is valid here because the gas is far enough from the liquid/vapor equilibrium to avoid the effects of fluid saturation.

The reactor model is thus complete and allows to account for its behavior during the decomposition phase as well as the synthesis phase by considering different parameters of the kinetic law for these 2 phases.

3.2. EMR of the other components of the thermochemical system

3.2.1. EMR of the condenser

It is assumed that the liquid level is the condenser is low and constant witch is the case when the condenser is placed directly above the tank and the liquid flows naturally to the tank by gravity. Moreover, the kinetics of the condensation is much higher than the kinetics of the chemical reaction. It is thus possible to consider that the condensation is instantaneous. From these 2 considerations, it assumed that there is no mass accumulation in the condenser since as soon as gas arrives it is instantly condensed and evacuated towards the liquid tank. Condenser wall have been neglected in this model because of their limited impact. Finally, the only energy accumulation in the condenser model is a thermal accumulation that sets the condensation temperature as a consequence of entropy flows from condensation and heat exchange with the heat transfer fluid. The complete diagram of the condenser model is available in Figure 6.

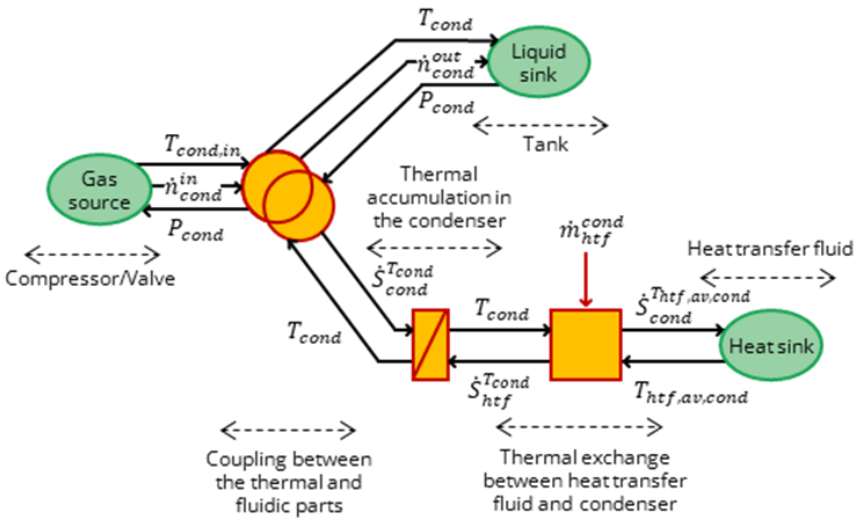

Variables		Subscripts and superscript	
T	Temperature	htf	Heat Transfer Fluid
P	Pressure	av	Average
$\dot{n}$	Molar flow rate	cond	Condenser
$\dot{S}$	Entropy flow	w	Wall
$\dot{m}$	Mass flow rate		

Figure 6 : EMR representation of the condenser. The meaning of each variable can be found using the nomenclature.

The coupling block between the thermal and fluidic part is simple because the gas and liquid molar flows are equal $\dot{n}_{cond}^{in} = \dot{n}_{cond}^{out}$ and the pressure is calculated from the saturation pressure at the condensation temperature $P_{cond} = P_{sat}(T_{cond})$. In order to calculate the entropy flow related to the production of heat due to condensation, an energy conservation balance can express the heat flow as shown in the equation (23). The entropy flux of condensation $\dot{S}_{cond}^{T_{cond}}$ is then deduced in a similar way to what was presented previously in equation (3).

$$\dot{S}_{cond}^{T_{cond}} = \frac{\Phi_{cond,htf}}{T_{cond}} = \frac{\dot{n}_{cond}^{in} \cdot \left(h_g(T_{cond,in}) - h_l(T_{cond})\right)}{T_{cond}} \quad (23)$$

In this equation h_g and h_l represents respectively the molar enthalpy of the gas and liquid phases and T_{cond} refers to the condensation temperature. The calculation of the condensation temperature, carried out in the accumulation bloc, is done by means of a heat balance on the condenser as shown in equation (24). In

this equation n_g is the number of moles of gas, n_l the number of moles of liquid, $c_{v,g}$ and $c_{v,l}$ are respectively the molar heat capacity at constant volume for the gas and the liquid phases, T_{cond} is the condensation temperature. $\dot{S}_{cond}^{T_{cond}}$ and $\dot{S}_{htf}^{T_{cond}}$ are respectively the two entropy fluxes due to the condensation of the gas and the heat exchange with the heat transfer fluid.

$$n_g . c_{v,g}(T_{cond}) + n_l . c_{v,l}(T_{cond}) . \frac{dT_{cond}}{dt} = \left(\dot{S}_{cond}^{T_{cond}} - \dot{S}_{htf}^{T_{cond}}\right) . T_{cond} \quad (24)$$

For the sake of simplicity, the heat accumulation in the condenser wall is neglected here. To take this into account, a heat exchange block between the condenser and the wall as well as an accumulation block should be added but the wall has little impact on the global dynamic of the system because the condenser is small ($0.5\ L$) and thus its wall mass is low compared to the thermal mass of the reactor.

For the heat exchange between the heat transfer fluid and the condenser, the overall heat exchange coefficient $(UA)_{cond}$ is calculated from a law extracted from the literature allowing to express it as a power law of the heat transfer fluid flow rate $\dot{m}_{htf}^{cond}$ as shown by equation (25). In the present case and considering the configuration of the exchanger, an exponent of 0.8 has been chosen. This coefficient must be adjusted according to the type of flow considered for the heat transfer fluid (laminar or turbulent) as well as according to the geometry of the exchanger. In this equation, the constant B will be identified from the different experimental data sets. The heat flux and the corresponding entropy flux are then calculated in the same way as presented in equations (5) and (3) respectively.

$$(UA)_{cond} = B . \left(\dot{m}_{htf}^{cond}\right)^{0.8} \quad (25)$$

3.2.2. EMR of the evaporator

The evaporator modeled here is a flooded type evaporator, i.e., constantly filled with liquid with only a slight gas overhead to ensure that a liquid/gas mixture remains present. To do this, the evaporator is placed under a small tank in which the liquid level is kept constant by means of a solenoid valve controlled by a level sensor. As for the condenser, the assumption of instantaneous evaporation remains valid because the kinetics

of evaporation is always much higher than the kinetics of the thermochemical reaction. As for the condenser, the wall is neglected here. These different considerations lead to consider that there is no mass accumulation block in the model but only a thermal accumulation block allowing to calculate the evaporation temperature. The EMR model of the evaporator is depicted in Figure 7.

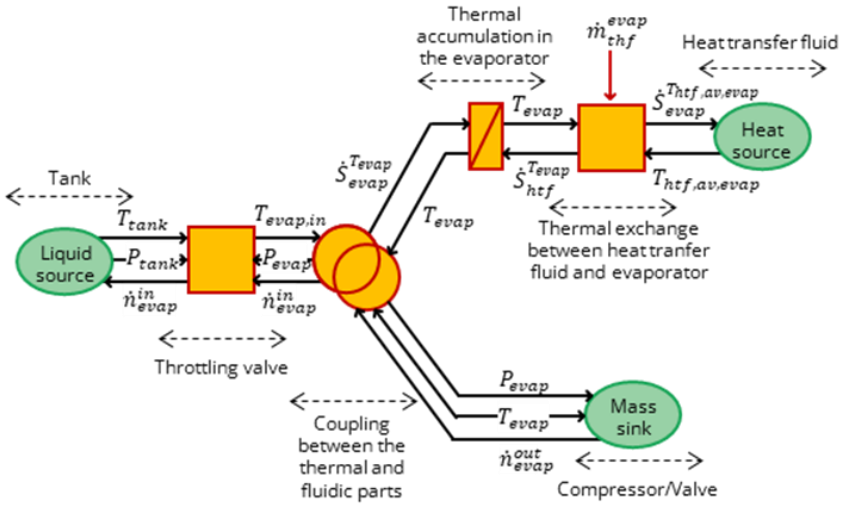

Variables		Subscripts and superscript	
T	Temperature	htf	Heat Transfer Fluid
P	Pressure	av	Average
$\dot{n}$	Molar flow rate	evap	Evaporator
$\dot{S}$	Entropy flow	w	Wall
$\dot{m}$	Mass flow rate		

Figure 7 : EMR of the evaporator.

The first block, on the left in Figure 7, represents the expansion of the liquid through the throttling valve. The temperature at the inlet of the valve T_{tank} is the temperature of the tank. The computation of the temperature at the outlet $T_{evap,in}$ is made with the knowledge of the pressure P_{evap} and the enthalpy $h(P_{tank}, T_{tank})$ because the expansion is supposed to be isenthalpic.

The coupling block between the thermal and fluidic part is quite similar to the condenser coupling bloc. The pressure is calculated by considering the pressure as the saturation pressure at the evaporation

temperature, both molar flow of gas and liquid are equal, and the entropy flow is computed thanks to an energy conservation balance in the evaporator.

The calculation of the evaporator temperature, carried out in the accumulation bloc, is done by means of a heat balance on the evaporator similarly to equation (24) for the condenser.

Finally, the thermal exchange between the heat transfer fluid and the evaporator $(UA)_{evap}$ is made with the identification of the constant parameter C which characterize the overall heat transfer coefficient as shown by equation (26). In this equation $\dot{m}_{htf}^{evap}$ refers to the mass flow rate of the heat transfer fluid at the evaporator.

$$(UA)_{evap} = C.\left(\dot{m}_{htf}^{evap}\right)^{0.8} \tag{26}$$

3.2.3. EMR of the mechanical compressor

The proposed EMR model is shown in Figure 8. The compressor is located between 3 sources or sinks, one gas sources at its inlet, one gas sink at its outlet and a mechanical energy source to drive it in rotation.

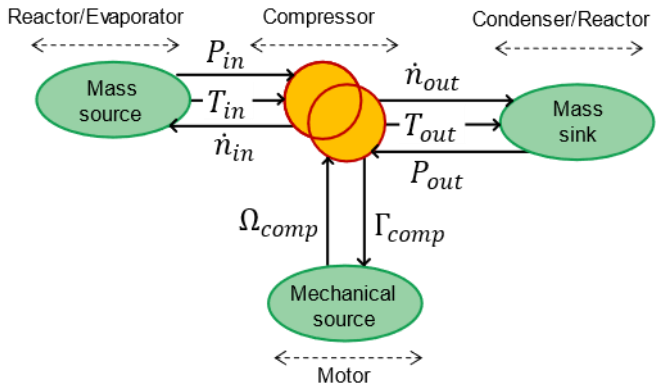

Variables		Subscripts and superscript	
T	Temperature	comp	Compressor
P	Pressure		
$\dot{n}$	Molar flow rate		
Ω	Rotation speed		
Γ	Torque		

Figure 8 : EMR of the compressor.

435 The molar flow rate entering the compressor $\dot{n}_{in}$ depends on the volumetric efficiency of the compressor
436 η_v, the swept volume per second $\dot{V}_b$ and the molar volume of the gas at the inlet of the compressor
437 $v_m(T_{in}, P_{in})$ as shown in equation (27).

$$\dot{n}_{in} = \frac{\eta_v . \dot{V}_b}{v_m(T_{in}, P_{in})} \tag{27}$$

438 The volumetric efficiency can be estimated from the knowledge of the adiabatic coefficient of the gas
439 under consideration γ and the ratio of dead volume V_{dv} to swept volume V_b expressed as $\varepsilon_{comp} = V_{dv}/V_b$ as
440 written by equation (28). In this equation P_{in} and P_{out} refers respectively to the inlet and outlet pressure of
441 the compressor.

$$\eta_v = 1 - \varepsilon_{comp} . \left(\left(\frac{P_{out}}{P_{in}} \right)^{\frac{1}{\gamma}} - 1 \right) \tag{28}$$

442 The volume swept each second can be expressed by equation (29). This is a function of the compressor
443 speed Ω_{comp}, the volume of a cylinder V_{cyl} and the number of chambers of compression N_c.

$$\dot{V}_b = \frac{1}{2.\pi} . V_{cyl} . N_c . \Omega_{comp} \tag{29}$$

444 Finally, the molar flow rate of gas drawn in by the compressor $\dot{n}_{in}$ can be obtained by equation (30).

$$\dot{n}_{in} = \left[1 - \varepsilon_{comp} . \left(\left(\frac{P_{out}}{P_{in}} \right)^{\frac{1}{\gamma}} - 1 \right) \right] . \frac{1}{2.\pi} . V_{cyl} . N_{cyl} . \Omega_{comp} . \frac{1}{v_m(T_{in}, P_{in})} \tag{30}$$

445 The outlet temperature can be estimated using the isentropic efficiency η_{is} of the compressor as shown
446 in equation (31). The isentropic efficiency will be considered constant as a first approximation. Knowing the
447 enthalpy and the discharge pressure it is thus possible to estimate the discharge temperature using
448 thermodynamic relations or tabulated values. In this equation h_{out}^{is} is the molar enthalpy of the gas at the
449 outlet of the compressor considering an isentropic compression, h_{in} is the molar enthalpy of the gas at the
450 inlet and h_{out} the real molar enthalpy of the gas at the outlet of the compressor.

$$\eta_{is} = \frac{h_{out}^{is} - h_{in}}{h_{out} - h_{in}} \quad (31)$$

In order to calculate the driving torque of the compressor Γ_{comp}, an energy conservation balance on the compressor shaft is performed as shown in equation (32) using the rotation speed of the compressor Ω_{comp}, the molar flow rate of the gas $\dot{n}_g$ and the molar enthalpy of the gas at the inlet h_{in} and outlet h_{out}.

$$\Gamma_{comp}.\Omega_{comp} = \dot{n}_g.(h_{out} - h_{in}) \quad (32)$$

3.2.4. Valve

The equations for calculating the flow through a valve depend on the flow regime. In the case of an expansion ratio greater than 2, we will consider that the flow is supersonic and that the flow rate is only a function of the upstream characteristics. Otherwise, the pressure difference ΔP between upstream P_{in} and downstream P_{out} must be considered in order to calculate the flow rate q_v. The two equations allowing to estimate the flow are given by equation (33) and (34). In this equation G_g is the specific density of the considered gas, C_v is the heat capacity at constant volume and N is a coefficient whose value depends on the units considered for the different quantities. With P in bar, q_v in std L/min and T in K, N is taken at 6950.

$$Subsonic\ \left(\frac{P_{in}}{P_{out}} < 2\right): \quad q_v = N.C_v.P_{in}.\left(1 - \frac{2.\Delta P}{3.P_{in}}\right).\sqrt{\frac{\Delta P}{P_{in}.G_g.T_{in}}} \quad (33)$$

$$Supersonic\ \left(\frac{P_{in}}{P_{out}} > 2\right): \quad q_v = 0.471.N.C_v.P_{in}.\sqrt{\frac{1}{G_g.T_{in}}} \quad (34)$$

3.3. EMR model for the whole hybrid thermochemical system

All the components of a thermochemical system have been modeled and implemented into *Simulink*. For the complete model of the hybrid thermochemical system, several flow distribution blocs have been designed for this purpose. These blocks allow to redirect the flows according to the considered phase (decomposition or synthesis) or to the use or not of a compressor. It can be noticed in this model, depicted on Figure 9, that two compressors are used but, in the real system, the same compressor could drive both decomposition and synthesis phase. This artifice allows to clarify the modeling of the complete system. This global model has 4

energy sources or sinks: 3 heat sources/sinks for the different heat transfer fluids (related to the reactor, condenser and evaporator) and one mechanical source to drive the compressor.

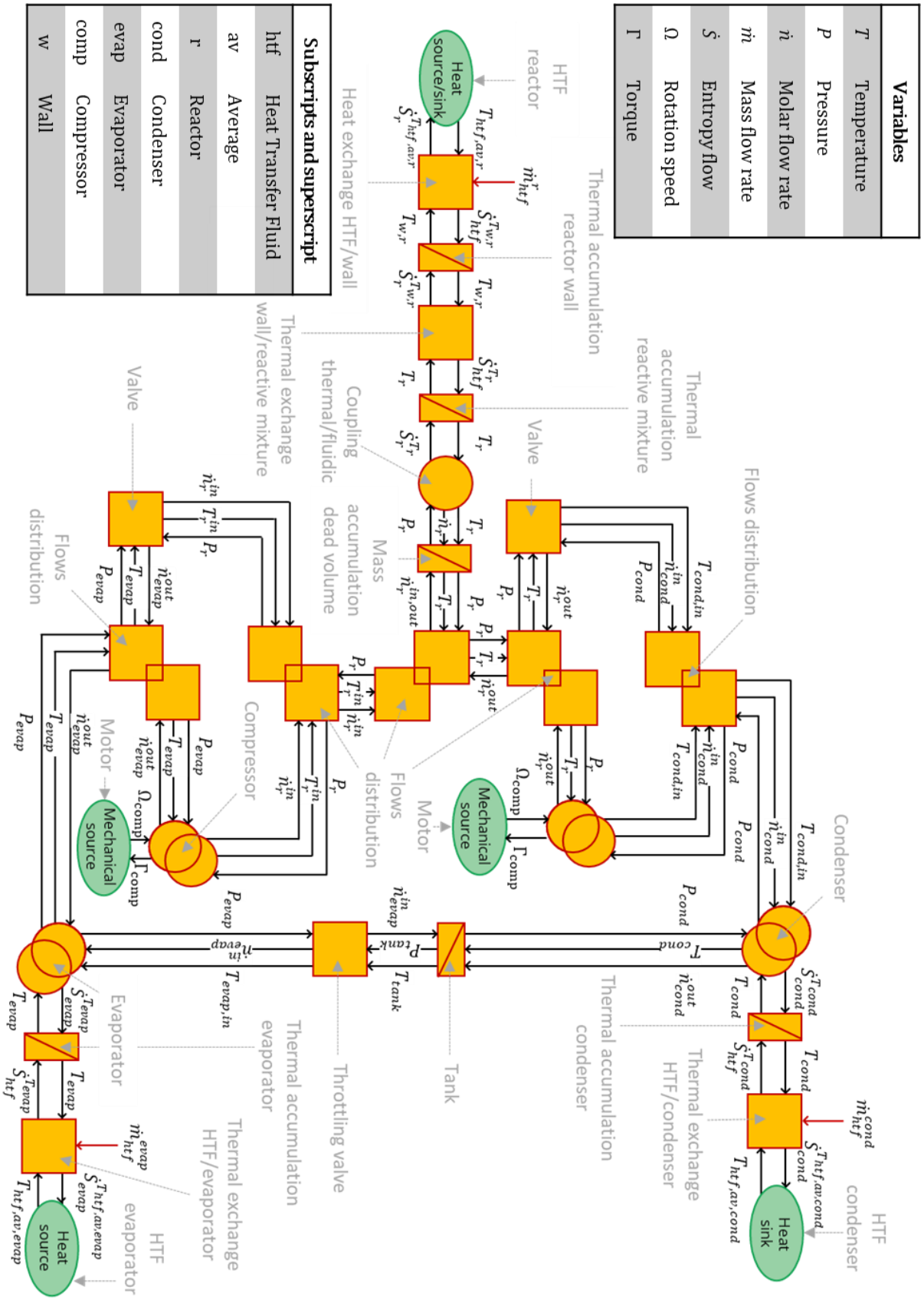

Figure 9 : EMR of the entire hybrid thermochemical system.

4. Experimentation and model validation

The prototype used to validate the model use the $BaCl_2$(8/0) salt which react with ammonia. This system is described in [19] and has been modified to be able to test the compressor-assisted synthesis phase, one dataset for each of the 4 phases was used to identify the model calibration parameters.

A system identification is made through a whitebox testing with a Particle Swarm Optimization (PSO) algorithm to tune the calibration parameters of the model to fit the experimental observations. The operation of this algorithm is described by Eberhart and Kennedy [27]. This algorithm is based on the generation of a particle swarm for which the position of each particle represents a possible solution to the optimization problem. The particles are then iteratively moved in the solution space to ensure a convergence towards a suitable solution to the optimization problem. This type of algorithm does not ensure to obtain the optimal solution in the mathematical sense of the term but an approximate solution which remains largely acceptable for this optimization problem. To estimate the degree of correlation between the model and the experimental observations the root mean square error (RMSE), defined by equation (35) is used. This indicator expresses the average distance between the experimental points and those obtained by simulation under the same operating conditions. In this equation, Val represents the value of the considered parameter either for the simulation Val^{sim} or for the experimentation Val^{exp}, n represents the different timesteps and N_f the total number of timesteps.

$$RMSE = \sqrt{\frac{\sum_{n=0}^{N_f}\left(Val^{sim}(n) - Val^{exp}(n)\right)^2}{N_f}} \tag{35}$$

Three representative variables of the thermochemical process operation are selected:

- the pressure in the reactor P_r
- the advancement of the reaction X
- the condensation pressure P_{cond} or the evaporation pressure P_{evap} depending on the operating phase considered.

The score of a particle for a given experiment is thus calculated as the sum of the RMSE for each of these 3 variables.

4.1. Model parameters

The input data for the modeling are the design parameters of the prototype (Table 2) and the operating conditions of the corresponding experiment:

- The temperatures of the heat transfer fluids at the reactor, condenser, and evaporator.
- The mass flow rates of the 3 heat transfer fluids.
- The rotation speed of the compressor when it is used.

Table 2 : Design parameter of the prototype used as input data of the model.

** These data come from values collected and computed by Touzain* [28] *and from CNRS-PROMES knowledge.*

*** Typical value of the average isentropic efficiency of a reciprocating compressor considering the operating condition of this study.*

	Parameter	Values
Reactor	Number of moles of salt n_s [8]	$64.9\ mol$
	ENG mass m_{ENG} [29]	$2.21\ kg$
	Wall of the tube reactor mass $m_{w,r}$ [29]	$25.7\ kg$
	Thermal capacity of the salt $c_{p,s,av}$ *	$76.8\ J.mol^{-1}.K^{-1}$
	Thermal capacity of the ENG $c_{p,ENG}$	$800\ J.kg^{-1}.K^{-1}$
	Thermal capacity of the tube reactor wall $c_{p,w,r}$	$502\ J.kg^{-1}.K^{-1}$
	Standard enthalpy of reaction $\Delta_r H°$ *	$38\ 248\ J.mol^{-1}.K^{-1}$
	Standard entropy of reaction $\Delta_r S°$ *	$232.4\ J.mol^{-1}$
Compressor	Isentropic efficiency η_{is}**	0.7
	Volume of the compression chamber V_{cyl} [30]	$0.345\ L$
	Number of cylinders N_{cyl} [30]	2

Condenser	Condenser volume V_{cond} [30]	$0.5\ L$
	Volume fraction of liquid $\gamma_{liq,cond}$	$1\ \%$
	Exchange area S_{cond} [30]	$0.35\ m^2$
Evaporator	Evaporator volume V_{evap} [30]	$0.5\ L$
	Volume fraction of liquid $\gamma_{liq,evap}$	$99\ \%$
	Exchange area S_{evap} [30]	$0.35\ m^2$

However, some parameters remain unknown or are simply difficult to estimate, such as kinetic coefficients, heat exchange coefficients or characteristics impacting the compressor operation. This set of unknown parameters constitute the calibration parameters of the model. A total of 9 parameters are used:

- 4 parameters for the kinetic relations. For each phase (decomposition and synthesis), 2 kinetic coefficients are needed: k_{kin} and n as stated in equation (20).
- 4 parameters for the overall heat transfer coefficient, as used in equations (6), (8), (25) and (26).
- 1 parameter for the ratio between the dead volume and the swept volume of the compressor, as characterized by equation (28).

By means of an optimization over the 4 operating phases, the values summarized in Table 3 are obtained for each of the calibration variables.

Table 3 : Identified values for the model calibration parameters.

Calibration variables	Nomenclature	Value
Kinetic decomposition coefficient	$k_{cin,dec}$	$1.10^{-3}s^{-1}$
Kinetic decomposition exponent	α_{dec}	$1.7\ [-]$
Kinetic synthesis coefficient	$k_{cin,synt}$	$1.10^{-3}s^{-1}$
Kinetic synthesis exponent	α_{synt}	$0.3\ [-]$
Overall heat transfer coefficient salt/wall	$(UA)_{reac,int}$	$524\ W.K^{-1}$
Overall heat transfer constant htf/wall	A	$2500\ [W.K^{-1}.kg^{-0.6}.s^{0.6}]$
Overall heat transfer constant condenser	B	$2500\ [W.K^{-1}.kg^{-0.8}.s^{0.8}]$
Overall heat transfer constant evaporator	C	$2800\ [W.K^{-1}.kg^{-0.8}.s^{0.8}]$
Dead volume to swept volume ratio compressor	ε_{comp}	$0.2\ [-]$

4.2. Comparison between numerical and experimental results

The results of the modeling of the prototype according to the 4 phases of operation are presented on Figure 10. The results concerning the validation of the model are presented as a distribution of the experimental and simulated data. The solid line represents a hypothetical model that should perfectly match the experimental observations. The pressure differences between the EMR model and the experiments are always lower than 1 bar, the advancement is accurately estimated because the error is never higher than 0.1 and the reactor wall temperature is never estimated with an error greater than 2 °C.

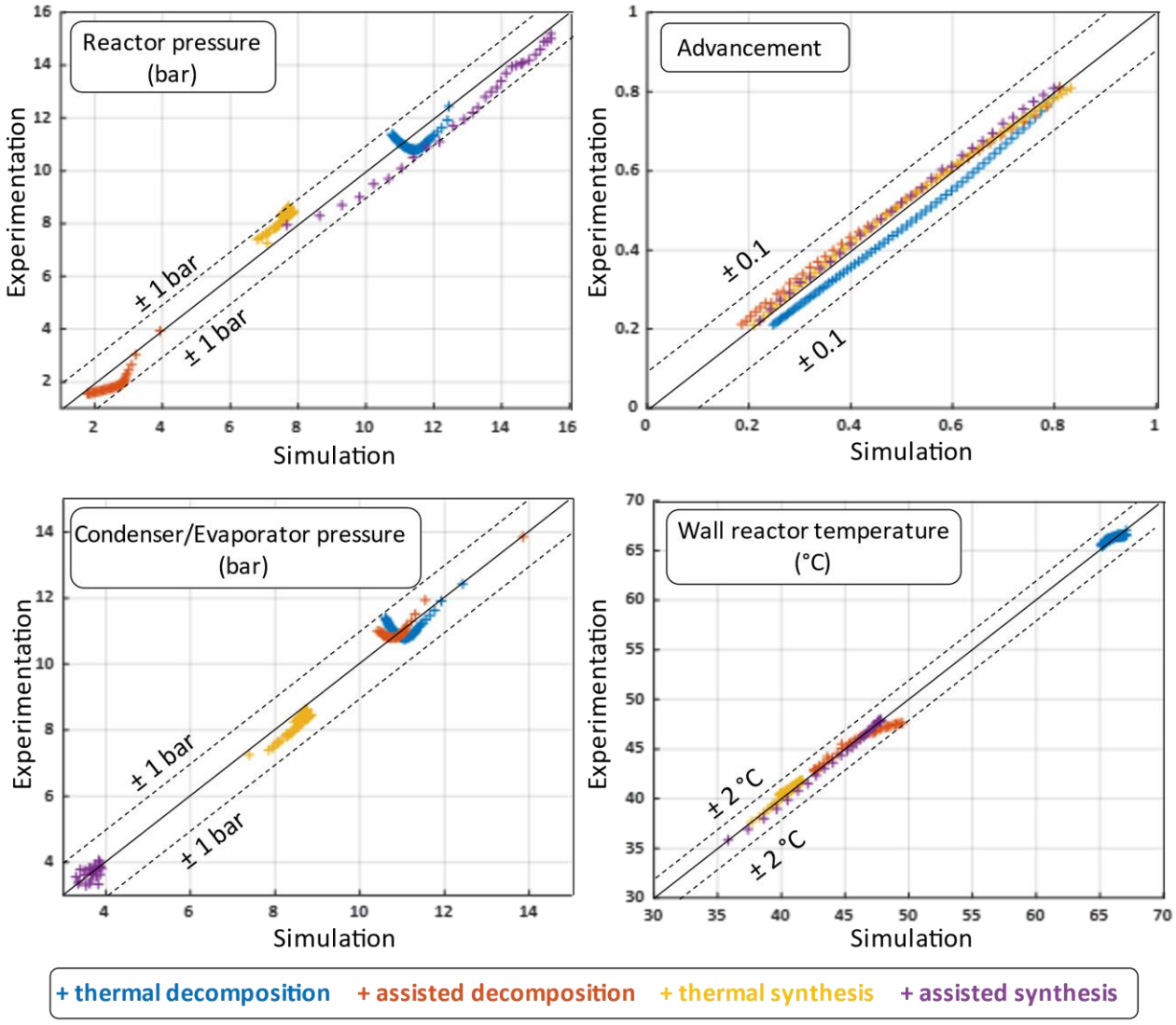

Figure 10 : Distributions of experimental and simulated results for reactor, condenser and evaporator pressure, feed rate and reactor wall temperature.

In order not to overload this article, the temporal evolutions of the different signals from the experiment or the simulation are not presented here but are visible in [8].

5. Application in process control

To understand the different potential applications offered by this EMR model, an example of temperature control of a cold room is proposed. The EMR model established previously allows, by inversion of the model, to drive the compressor in synthesis phase to control the temperature of a cold load. The integration of a compressor in the thermochemical process allows to reach temperatures close to -30 °C, the application considered here is the regulation during 24 h of the temperature of a negative cold room at -18 °C, common temperature considered for freezing applications. An illustration of the thermochemical process implemented for this purpose is proposed and represented in Figure 11 in the cold production mode.

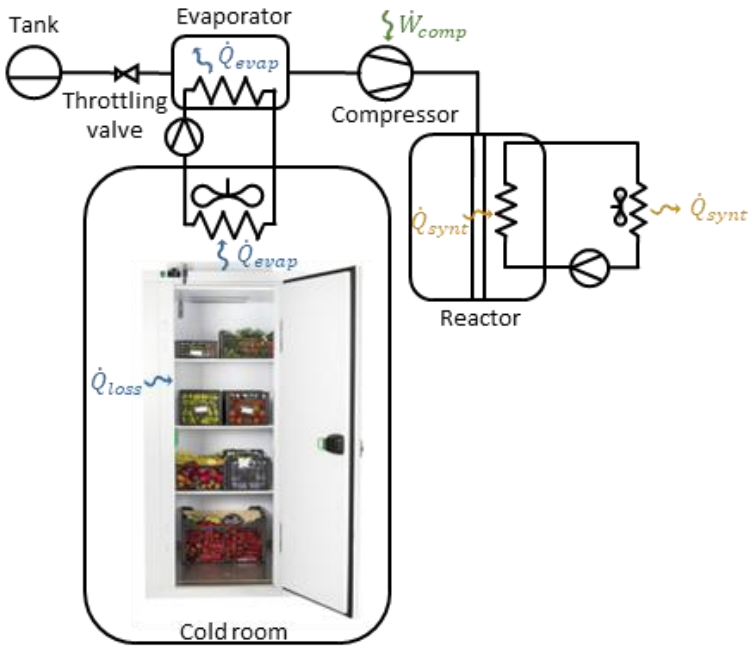

Figure 11 : Scheme of the proposed process control for the regulation of a cold room temperature.

To model the thermal loads of the cold room during a day, a classical loss profile is used. This one has been scaled to match the total energy lost during the day with the type of cold room used for this study. The energy loss of the cold room over a day is calculated by considering the losses by conduction, the openings of the

door as well as the introduction of food in the cold room. The whole calculation is detailed in [8]. The curve representing the heat loads of the cold room during a day is shown in Figure 12.

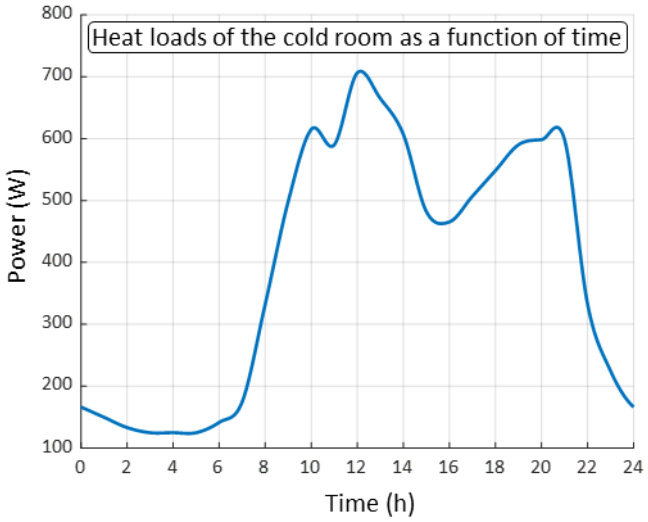

Figure 12 : Heat loads from the cold room on a typical day.

As stated before, a model inversion must be performed to obtain a control structure allowing to drive the compressor to control and regulate the temperature of the cold room. This inversion can be seen as an inversion of the physical functionality of the system. A causal relationship, also often called control chain for this type of modeling, correspond to a series of parameters to be set to go from the control variable (compressor speed) to the variable to be controlled (cold room temperature). This relation must be defined from the model in function of the control the user wants to apply. This causal relationship is then inverted to obtain a command chain to determine the control law of the compressor speed versus the cold room temperature. This methodology allows us to identify the blocks that need to be inverted as well as the variables to be controlled. These two chains, as well as the EMR model and its inversion are presented in Figure 13.

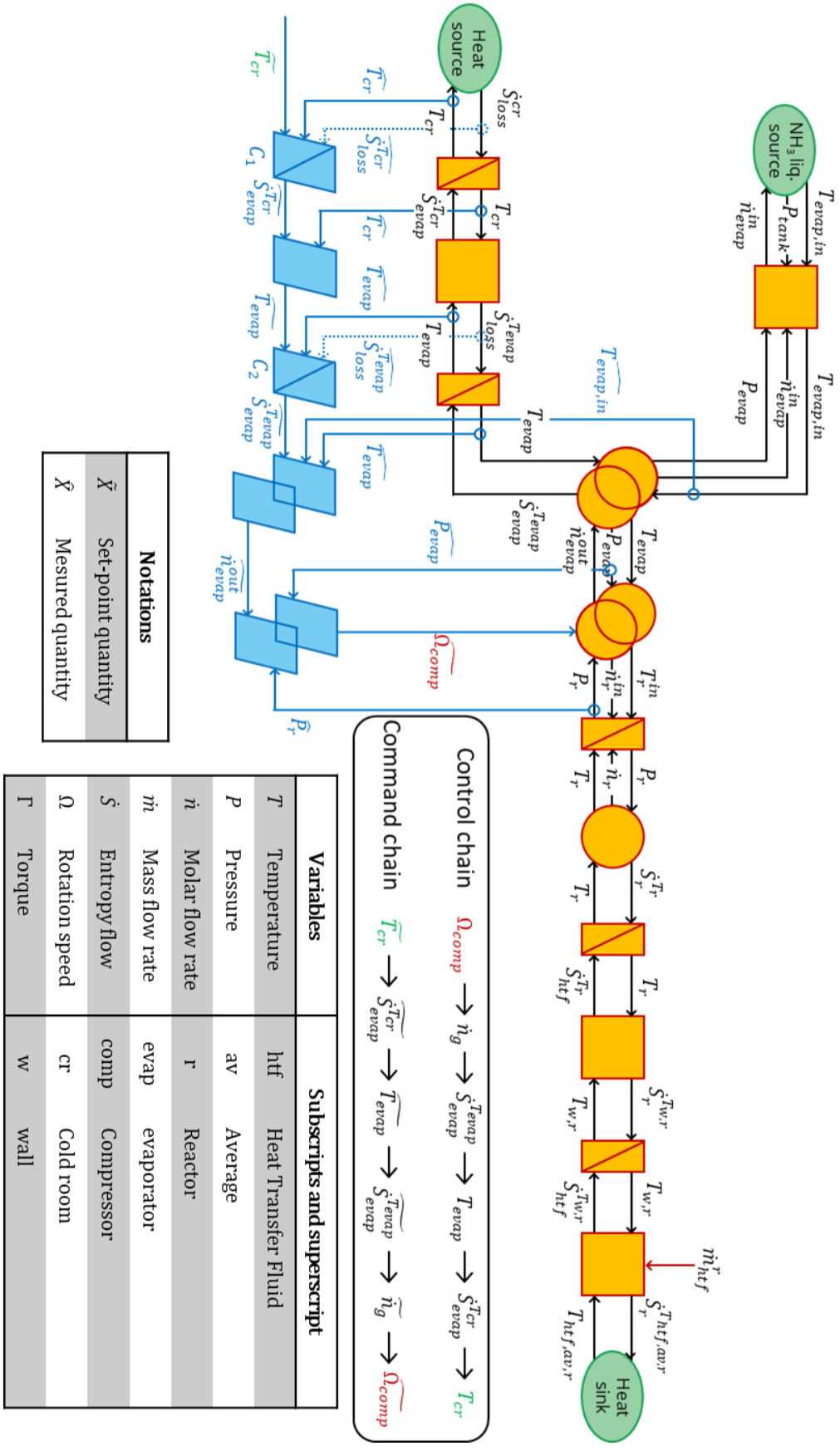

Figure 13 : EMR model of the control process and inversion of the causal relationship.

In Figure 13, the "tilde" notations refer to set-point quantities that are found in the chain of causal relations, while the "circumflex" notations refer to measured quantities. The control structure obtained by inversion of the EMR model is called the maximum control structure. This structure can then be simplified to reduce the number of measurements to be performed on the system. This step is not detailed here because the objective is not to actually implement the control strategy obtained. However, the dotted lines in Figure 13 refer to the quantities that should be removed because they are difficult to measure. To do this, a more robust PI type corrector could be used to eliminate the need to measure these quantities.

The method used for the inversion of each block is described by Walter *et al.* [9]. Three types of blocks are involved in the causal relationship: two accumulation blocks, a monophysical coupling block and two multiphysical conversion blocks. The inversion reveals two correctors that need to be adjusted.

As the control loops are nested, it is essential that the time constants, chosen from the parameters of the correctors, are consistent with each other so that the internal loop is faster than the external loop. To simplify the adjustment, the correctors used proportional type. Their respective gains were manually adjusted to obtain an internal control loop whose response time is about 10 times less than the external loop. For this reason, the gain of the C1 corrector is equal to 1 and that of C2 to 10.

To facilitate the understanding of the control strategy of the system, Figure 14 represents the regulation in a more conventional way by means of a block diagram.

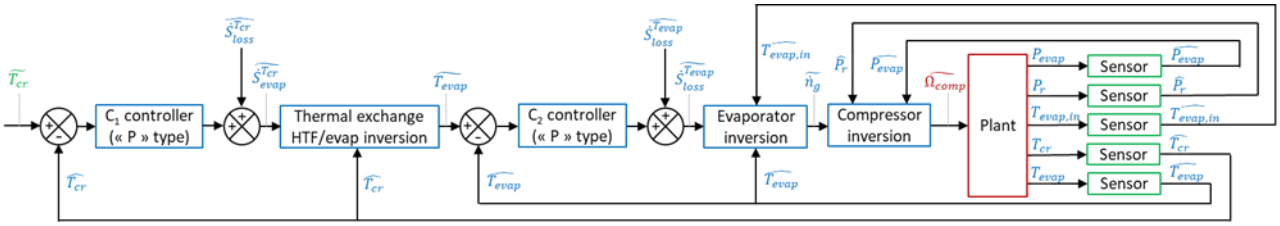

Variables		Subscripts and superscript		Notations	
T	Temperature	htf	Heat Transfer Fluid	$\tilde{X}$	Set-point quantity
P	Pressure	av	Average	$\hat{X}$	Mesured quantity
$\dot{n}$	Molar flow rate	r	Reactor		
$\dot{m}$	Mass flow rate	evap	evaporator		
$\dot{S}$	Entropy flow	comp	Compressor		
Ω	Rotation speed	cr	Cold room		
Γ	Torque	w	wall		

Figure 14 : Block diagram representation of the control structure.

The geometrical and thermodynamic parameters considered are those of the prototype described earlier except for the number of reactive tubes which has been increased to 21 instead of 7. The exchange surfaces, the mass of the walls, the reactive composite and the dead volume have been modified accordingly. The ambient temperature is considered constant and equal to 25 °C.

The results obtained are described in Figure 15. It can be seen that the objective is reached, the temperature of the cold room can be maintained at -18 °C for 24 hours by adapting the rotation speed of the compressor. We also see that the choice to use 21 reactive tubes instead of 7 is justified because the synthesis reaction is complete at the end of the day (X≃1). Nevertheless, we notice that the compressor, although it is one of the smallest powers available on the market, is here oversized compared to the refrigeration load of the cold chamber: its rotation speed is too low to ensure a correct lubrication of it. It would therefore be necessary to make it rotate at a higher speed which is suitable for the compressor (about 35% of its nominal speed, as recommended by the manufacturer) and to use a by-pass to reinject part of the compressed vapors from the discharge to the suction. Note that this type of capacity modulation is not very energy efficient.

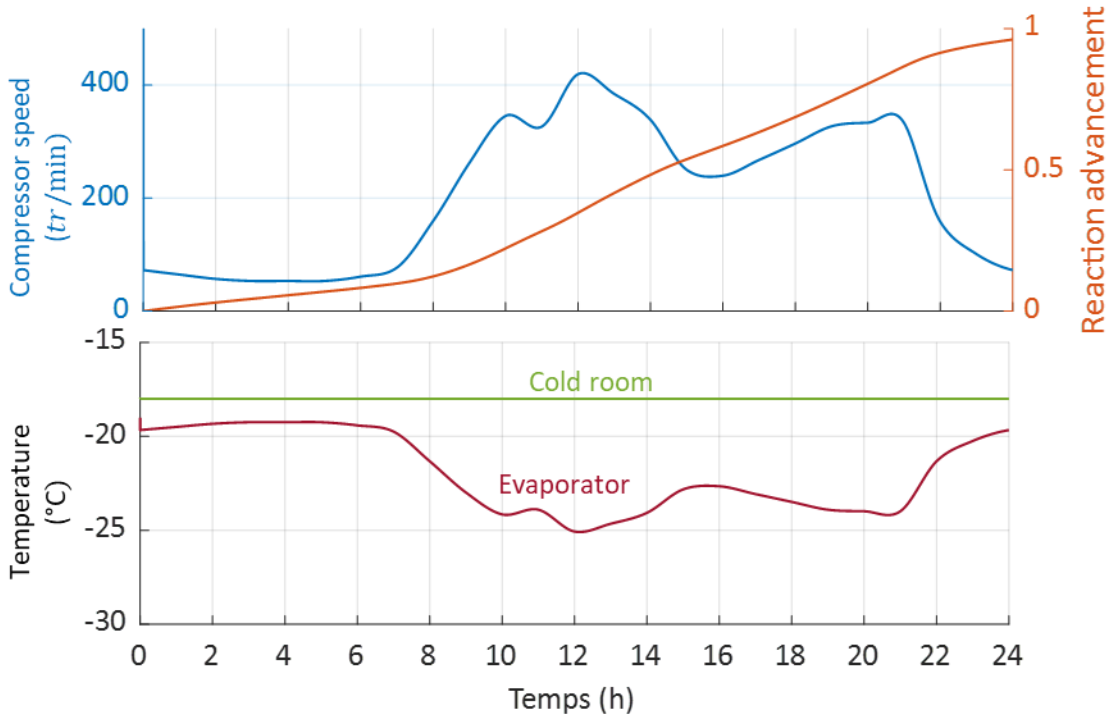

593

594 *Figure 15 : Results for cold room temperature regulation based on compressor speed control.*

595 **6. Conclusion**

596 The compression-assisted hybrid thermochemical cooler studied in this article make it possible to use heat
597 sources at lower temperatures or to produce cold at lower temperatures than conventional thermochemical
598 cooler. In addition, the presence of a variable-speed mechanical compressor in the process provides an extra
599 degree of freedom for process control. The study described in this article proposes a methodology to defined
600 control structures for these innovative thermochemical processes. This investigation allows to bring
601 thermochemical systems closer to an industrial development which would allow this type of system to find its
602 place in the energy transition.

603 The contributions and main conclusions of this study are as follows:

- development of models of thermodynamic machine components (thermochemical reactor, compressor, evaporator, condenser, expansion valve) in the EMR formalism. These component models could be used in the future to model other thermodynamic machines using the EMR formalism.

- development of a complete model of a mechanical compression-assisted thermochemical process with the EMR formalism. The unknown parameters of this model have been identified thanks to a PSO algorithm and the model has been validated by comparison with experimental data obtained from a highly instrumented prototype. Deviation between numerical and experimental data are lower than $1\ bar$ for the reactor, condenser and evaporator pressure, lower than 0.1 for the reaction advancement and lower than $2\ °C$ for the reactor wall temperature. This validated model can easily be used to study couplings between thermochemical refrigerators and processes previously modeled with the EMR formalism (e.g. electrolyzer, fuel cell...).

- the inversion of the process model has enabled to establish a process control law. An application is described to show how the compressor speed can be set to maintain a cold room at $-18\ °C$ despite significant load variations (from $120\ W$ to $700\ W$). Simulations showed that compressor speed control enabled the cold room temperature to be maintained with a maximum difference of $1\ °C$ from the set temperature.

- the inversion method of the EMR model could be used to implement control chain of the coupling between thermochemical refrigerators and processes previously modeled with the EMR formalism (e.g. electrolyzer, fuel cell...).

Acknowledgments

This work was supported by the French National Research Agency (ANR) in the framework of the RECIF project under contract ANR-18-CE05-0043 (https://anr.fr/Projet-ANR-18-CE05-0043). These studies have been conducted within the PROMES laboratory which the authors would like to thank too. The prototype used for the validation of the model has been developed at the University of French Polynesia.

7. Bibliography

[1] C. Forman, I. K. Muritala, R. Pardemann, and B. Meyer, "Estimating the global waste heat potential," *Renew. Sustain. Energy Rev.*, vol. 57, pp. 1568–1579, 2016, doi: 10.1016/j.rser.2015.12.192.

[2] L. Jiang, R. Q. Wang, X. Tao, and A. P. Roskilly, "A hybrid resorption-compression heat transformer for energy storage and upgrade with a large temperature lift," *Appl. Energy*, vol. 280, p. 115910, 2020, doi: 10.1016/j.apenergy.2020.115910.

[3] L. Jiang, S. Li, R. Q. Wang, Y. B. Fan, X. J. Zhang, and A. P. Roskilly, "Performance analysis on a hybrid compression-assisted sorption thermal battery for seasonal heat storage in severe cold region," *Renew. Energy*, vol. 180, pp. 398–409, 2021, doi: 10.1016/j.renene.2021.08.101.

[4] K. S. Babu and E. A. Kumar, "Thermodynamic analysis of compressor operated resorption thermochemical energy storage system for heat storage , combined cooling and heat upgradation," *J. Energy Storage*, vol. 50, p. 104659, 2022, doi: 10.1016/j.est.2022.104659.

[5] G. Zisopoulos, A. Nesiadis, K. Atsonios, N. Nikolopoulos, D. Stitou, and A. Coca-Ortegón, "Conceptual design and dynamic simulation of an integrated solar driven thermal system with thermochemical energy storage for heating and cooling," *J. Energy Storage*, vol. 41, 2021, doi: 10.1016/j.est.2021.102870.

[6] P. Gao, L. W. Wang, and F. Q. Zhu, "Vapor-compression refrigeration system coupled with a thermochemical resorption energy storage unit for a refrigerated truck," *Appl. Energy*, vol. 290, p. 116756, 2021, doi: 10.1016/j.apenergy.2021.116756.

[7] P. Gao, X. Wei, L. Wang, and F. Zhu, "Compression-assisted decomposition thermochemical sorption energy storage system for deep engine exhaust waste heat recovery," *Energy*, vol. 244, p. 123215, 2022, doi: 10.1016/j.energy.2022.123215.

[8] A. Perrigot, "Cycles hybrides thermochimiques à compression. Application aux micro-réseaux

autonomes de cogénération électricité/froid.," Université de Perpignan Via Domitia, 2022.

[9] L. Walter, D. Philippe, B. Alain, and B. Philippe, "La REM, formalisme multiphysique de commande de systèmes énergétiques," *Tech. l'ingénieur Outil. d'analyse en électronique puissance métrologie*, vol. base docum, no. ref. article : d3066, 2014, [Online]. Available: https://www.techniques-ingenieur.fr/base-documentaire/energies-th4/outils-d-analyse-en-electronique-de-puissance-et-metrologie-42278210/la-rem-formalisme-multiphysique-de-commande-de-systemes-energetiques-d3066/

[10] K. S. Agbli, D. Hissel, M. C. Péra, and I. Doumbia, "Energetic Macroscopic Representation (EMR): New approach for multiphysics energetic flows modelling," *IFAC Proc. Vol.*, vol. 8, pp. 723–728, 2012, doi: 10.3182/20120902-4-fr-2032.00126.

[11] W. Lhomme, A. Bouscayrol, and P. Barrade, "Simulation of a series hybrid electric vehicle based on energetic macroscopic representation," *IEEE Int. Symp. Ind. Electron.*, vol. 2, pp. 1525–1530, 2004, doi: 10.1109/ISIE.2004.1572040.

[12] P. Delarue, A. Bouscayrol, A. Tounzi, and X. Guillaud, "Modelling , control and simulation of an overall wind energy conversion system," *Renew. Energy*, vol. 28, pp. 1169–1185, 2003, doi: 10.1016/S0960-1481(02)00221-5.

[13] J. C. Mercieca, J. N. Verhille, and A. Bouscayrol, "Energetic Macroscopic Representation of a Subway Traction System for a Simulation Model," *IEEE Int. Symp. Ind. Electron.*, vol. 2, pp. 1519–1524, 2004.

[14] L. Horrein, A. Bouscayrol, Y. Cheng, and M. El Fassi, "Dynamical and quasi-static multi-physical models of a diesel internal combustion engine using Energetic Macroscopic Representation," *Energy Convers. Manag.*, vol. 91, pp. 280–291, 2015, doi: 10.1016/j.enconman.2014.12.022.

[15] C. Gay, F. Lanzetta, D. Hissel, and M. Feidt, "Représentation Energétique Macroscopique (REM) d'un moteur Stirling en vue d'une hybridation thermique," *Société Française Therm.*, no. November 2014, pp. 1–6.

[16] K. S. Agbli, M. Pera, D. Hissel, O. Rallières, C. Turpin, and I. Doumbia, “Multiphysics simulation of a PEM electrolyser : Energetic Macroscopic Representation approach,” *Int. J. Hydrogen Energy*, vol. 6, pp. 1382–1398, 2011, doi: 10.1016/j.ijhydene.2010.10.069.

[17] D. Chrenko and P. Marie-Cécile, “Energetic Macroscopic Representation Modeling and Control of a Low Temperature Fuel Cell System Fed by Hydrocarbons,” 2008, [Online]. Available: https://tel.archives-ouvertes.fr/tel-00358312

[18] P. Neveu, “Diagrammes thermodynamiques relatif aux équilibres solide/gaz.” 1996.

[19] F. Ferrucci, D. Stitou, P. Ortega, and F. Lucas, “Mechanical compressor-driven thermochemical storage for cooling applications in tropical insular regions. Concept and efficiency analysis,” *Appl. Energy*, vol. 219, pp. 240–255, 2018, doi: 10.1016/j.apenergy.2018.03.049.

[20] J. Fitó, A. Coronas, S. Mauran, N. Mazet, M. Perier-Muzet, and D. Stitou, “Hybrid system combining mechanical compression and thermochemical storage of ammonia vapor for cold production,” *Energy Convers. Manag.*, vol. 180, pp. 709–723, 2019, doi: 10.1016/j.enconman.2018.11.019.

[21] A. Perrigot, M. Perier-muzet, P. Ortega, and D. Stitou, “Thermodynamic performance ’ s analysis of a cold production by hybrid compressor-based thermochemical sorption processes using ammoniated salts,” *Energy Convers. Manag.*, vol. 267, 2022.

[22] H. B. Lu, N. Mazet, and B. Spinner, “Modelling of gas-solid reaction - Coupling of heat and mass transfer with chemical reaction,” *Chem. Eng. Sci.*, vol. 51, no. 15, pp. 3829–3845, 1996, doi: 10.1016/0009-2509(96)00010-3.

[23] L. Hui-Bo, N. Mazet, O. Coudevylle, and S. Mauran, “Comparison of a general model with a simplified approach for the transformation of solid-gas media used in chemical heat transformers,” *Chem. Eng. Sci.*, vol. 52, no. 2, pp. 311–327, 1997, doi: 10.1016/S0009-2509(96)00407-1.

[24] D. Stitou, V. Goetz, and B. Spinner, “A new analytical model for solid-gas thermochemical reactors based on thermophysical properties of the reactive medium,” *Chem. Eng. Process. Process Intensif.*,

698 vol. 36, no. 1, pp. 29–43, 1997, doi: 10.1016/S0255-2701(96)04173-6.

699 [25] P. Neveu and J. Castaing-Lasvignottes, “Development of a numerical sizing tool for a solid-gas
700 thermochemical process,” *Appl. Therm. Eng.*, vol. 17, no. 6, pp. 501–518, 1997.

701 [26] N. Mazet, M. Amouroux, and B. Spinner, “Analysis and experimental study of the transformation of a
702 non-isothermal solid/gas reacting medium,” *Chem. Eng. Commun.*, vol. 99, no. 1, pp. 155–174, 1991,
703 doi: 10.1080/00986449108911585.

704 [27] J. Kennedy and R. Eberhart, “Particle swarm optimization,” in *Proceedings of ICNN’95 - International*
705 *Conference on Neural Networks*, IEEE, 1995, pp. 1942–1948. doi: 10.1109/ICNN.1995.488968.

706 [28] P. Touzain, “Thermodynamic values of ammonia-salts reactions for chemical sorption heat pumps.,” in
707 *Proceedings of the international sorption heat pump conference, Munich, Germany. 1999*, 1999.

708 [29] N. Le Pierres, “Procédé solaire de production de froid basse température (-28 ° C) par sorption solide-
709 gaz Nolwenn Le Pierrès To cite this version : HAL Id : tel-00011253,” 2005.

710 [30] F. Ferrucci, “PV-driven vapor compression cycle integrating a solid-gas thermochemical storage for
711 cooling applications,” 2020.

712